PRAMANA — journal of physics

Vol. 76, No. 4
April 2011
pp. 639–656

Magnetic behaviour of AuFe and NiMo alloys

PRASHANT SINGH[1], RUDRA BANERJEE[1], MOSHIOUR RAHAMAN[2,5], A V RUBAN[2], BIPLAB SANYAL[3] and ABHIJIT MOOKERJEE[4,*]

[1]Department of Materials Sciences, S.N. Bose National Centre for Basic Sciences, JD Block, Sector III, Salt Lake City, Kolkata 700 098, India
[2]Applied Material Physics, Kungliga Tekniska Högskolan (Royal Institute of Technology), Valhallav 79, SE-100 44 Stockholm, Sweden
[3]Division of Materials Theory, Department of Physics and Materials Science, Angstromlaboratoriet, Uppsala University, Box 530, 75121 Uppsala, Sweden
[4]Advanced Materials Research Unit and Department of Materials Sciences, S.N. Bose National Centre for Basic Sciences, JD Block, Sector III, Salt Lake City, Kolkata 700 098, India
[5]Permanent address: S.N. Bose National Centre for Basic Sciences, JD Block, Sector III, Salt Lake City, Kolkata 700 098, India
*Corresponding author. E-mail: abhijit@bose.res.in

MS received 15 July 2010; revised 22 September 2010; accepted 1 October 2010

Abstract. We study the electronic structure and a mean-field phase analysis based on the pair–pair energies derived from first-principles electronic structure calculations of AuFe and NiMo alloys. We have used the tight-binding linear muffin-tin orbitals-based augmented space recursion (TB-LMTO-ASR) method to do so. We investigate different behaviours of the two alloy systems by mapping the problems onto equivalent Ising models and then discuss the magnetic phase diagrams using the calculated pair energies. All three phases: paramagnetic, random ferromagnetic and spin glass, have been studied.

Keywords. Alloys; magnetism; spin-glasses.

PACS Nos 75.10-b; 75.50.Lk; 75.10.Nr; 71.23.-k

1. Introduction

The magnetic behaviour of disordered alloys in which a magnetic component is diluted with a nonmagnetic one, or in which the components have competing ferro- and antiferromagnetic behaviour, has been the subject of intense research for a long time [1]. By now the experimental picture is well understood. In particular, it is understood that in certain composition ranges one finds a phase in which there is no long-ranged magnetic order, although magnetic moments exist locally. The susceptibility as a function of temperature shows a

characteristic cusp, indicating freezing of magnetic degrees of freedom. In the same 'spin-glass' phase, one observes history dependence and anomalously slow relaxation, which are characteristics of glassy materials.

In this work we shall examine two alloys, namely AuFe and NiMo. These alloys can be prepared in the disordered phase by fast quenching from the melt. Their magnetic behaviours are very different. AuFe is the archetypal 'spin-glass' which shows a spin-glass phase at low Fe compositions and random ferromagnetism in the Fe-rich regions. NiMo, on the other hand, shows random ferromagnetism in the Ni-rich region, but loses magnetism altogether as Mo concentration increases. It does not seem to exhibit a spin-glass phase. The aim of this communication, from a first-principles density functional-based theory, is to map the problem onto an equivalent Ising model and describe the magnetic phases from the calculated pair energies of the model.

Although such alloy phases have been quite exhaustively studied by techniques of both equilibrium and non-equilibrium statistical mechanics, a first-principles, microscopic study based on realistic models of such systems will throw light on the suitability of some of the underlying assumptions of the simplified solvable models as well as differences in behaviour because of local chemistry.

Successful mean-field approaches to the problem of spin-glasses vary from that of Sherrington–Kirkpatrick [2] to the sophisticated replica symmetry breaking ideas of Parisi [3,4]. Different ways of describing and dealing with the randomness were suggested by Kaneyoshi [5], Plefka [6], Thouless *et al* [7] and the virial expansion of Morita and Horiguchi [8]. The virial expansion is valid either at low or very high temperatures [9] or when the spin pair energy parameter $J \sim O(N^{-1/2})$. It is, in fact, invalid in the parameter range and coupling type of our interest. Most of these 'solvable' models assume specific type of spin pair energies like infinitely weak, infinitely long-ranged ($J \sim O(1/N)$) and further assume Gaussian distribution of these pair energies in an *ad hoc* manner. It would be interesting to examine these simplified models in the light of our first-principles analysis.

The paper is arranged as follows: in §2 we present the electronic structure of AuFe and NiMo disordered alloys at varying compositions and extract information about the density of states and local magnetic moment. In §3 we shall use our electronic structure and the generalized perturbation expansion formalism to map the problem of emergence of magnetic order onto a classical Ising model and obtain the effective pair energies. We shall examine the nature of these pair energies in detail. Finally, in §4 we shall use our mapped random Ising model to examine the phase diagram based on our analysis on mean-field theories.

2. Electronic structure of AuFe and NiMo

Our starting point will be the Kohn–Sham equation for the motion of electrons in the alloy. We can choose any method for generating Hamiltonians from first principles in which the basis is labelled by lattice points. Such a 'tight-binding' description is ideal for describing the substitutional disorder in the alloys of our interest. We shall choose the tight-binding, linear muffin-tin orbitals (TB-LMTO) method [10]. The TB-LMTO method is a standard technique by now and we shall refer the interested reader to the

above reference for details. In a random alloy the LMTO 'potential' parameters are random and we shall have to describe the properties of the system from the viewpoint of configuration averaging. Extensive work on methods dealing with configuration averaging exists. An extended discussion on the successful averaging techniques and a comparison between their estimates (for FeCr) is given in a recent paper by Tarafder *et al* [11]. In the present work we have chosen the augmented space recursion (ASR) [12] introduced by one of us.

The augmented space formalism deals with configurational averaging going beyond mean-field approaches like the CPA. It takes into account the effect of configurational fluctuations of the immediate neighbourhood of a site and can deal with inhomogeneous disorder like clustering [13], short-ranged ordering [14,15] and local distortions arising out of the size mismatch of the constituents [16]. The augmented space formalism is exact and approximations arise only in the recursion part. Recursion expands the configuration-averaged Green function as a continued fraction and the approximation is in the number of continued fraction steps accurately calculated before the asymptotic part is 'terminated' by one of the terminators suggested by Haydock [17] or Beer and Pettifor [18]. We shall terminate with the Beer–Pettifor terminator after 11 steps of recursion. This will mean that 20 moments of the density of states will be accurate, compared with only 8 moments in the CPA. The other major source of error is in the atomic sphere approximation of the TB-LMTO. One way out is to replace the TB-LMTO with full-potential LMTO. But then the Hamiltonian will no longer be sparse and recursion will lose accuracy. We shall stick with the TB-LMTO-ASR. The limit of accuracy of the total energy calculations is about ∼5–10 mRyd/atom. For energy differences less than this, our statements will be qualitative.

The calculations are LSDA-self-consistent and the Madelung energy is constructed according to the ideas of Ruban and Skriver [19]. Their screening parameters were obtained using the SQS technique as suggested by Ruban *et al* [20]. Within the TB-LMTO procedure, the solid is partitioned into atom centric atomic spheres (AS) labelled by $\vec{R}_i$. $\Phi(\vec{r} - \vec{R}_i)$ is the wave function projected in an AS at $\vec{R}_i$. Once we have calculated the configuration-averaged Green function $\langle\langle G^{\sigma}_{\vec{R}_i L, \vec{R}_i, L}(E)\rangle\rangle$ we immediately obtain the following local spin-resolved density of states:

$$n^{\sigma}(E, \vec{R}_i) = -\frac{1}{\pi}\Im m \mathrm{Tr}_L \langle\langle G^{\sigma}_{\vec{R}_i L, \vec{R}_i L}(E + i0^+)\rangle\rangle. \tag{1}$$

The charge and the magnetization densities are

$$\begin{aligned}
\rho^{\sigma}(\vec{r} - \vec{R}_i) &= \int_{-\infty}^{E_{\mathrm{F}}} |\Phi(\vec{r} - \vec{R}_i)|^2 n^{\sigma}(E, \vec{R}_i), \\
\rho(\vec{r} - \vec{R}_i) &= \rho^{\uparrow}(\vec{r} - \vec{R}_i) + \rho^{\downarrow}(\vec{r} - \vec{R}_i), \\
m(\vec{r} - \vec{R}_i) &= \rho^{\uparrow}(\vec{r} - \vec{R}_i) - \rho^{\downarrow}(\vec{r} - \vec{R}_i)
\end{aligned} \tag{2}$$

and the magnetic moment within an atomic sphere (AS) is

$$m(\vec{R}_i) = \int_{\mathrm{AS}} \mathrm{d}^3\vec{r} m(\vec{r} - \vec{R}_i),$$

where $\rho(\vec{r} - \vec{R}_i)$ is the charge density and $m(\vec{r} - \vec{R}_i)$ is the magnetic moment density in AS at $\vec{R}_i$. From this description it is clear that the magnetic moment is not localized at $\vec{R}_i$ but smeared across the AS. $m(\vec{R}_i)$ integrated over an AS is the average magnetic moment associated with it. These magnetic moments are thus built out of the itinerant electron charge densities associated with different spins.

Figure 1 shows the atom and spin projected density of states for $Au_{1-x}Fe_x$ at two characteristic compositions $x = 0.04$ and 0.10. This is an example of an almost split-band alloy with the Au and Fe spectra hardly overlapping each other. It was argued earlier that dilute split-band alloys are well described by the augmented space recursion technique used by us.

We first note that the Au densities of states are negligibly exchange-split. The Au atoms carry negligible magnetic moments at all compositions. The Fe density of state for the dilute Fe composition ($x = 0.04$) resembles a narrow impurity band for both the spin orientations. As the iron concentration increases the Fe PDOS becomes wider. The up-channel is almost fully occupied, while the down-channel is almost half full. This feature remains unchanged across the composition range.

Figure 2 shows the local magnetic moment on the Fe atom in the $Au_{1-x}Fe_x$ alloy in the same composition range. We should note two specific points:

(i) Even in the composition range $x \leq 0.1$, where the global magnetic moment is experimentally found to be zero, locally Fe atoms in the alloy have finite moments at low temperatures. The study of the local magnetic moment cannot distinguish the random ferromagnet from a spin-glass phase.

(ii) The local magnetic moment on Fe increases as its concentration decreases. This indicates that the magnetism on Fe is predominantly itinerant. We have noted that the projected density of states for Fe becomes narrower as its concentration decreases. The Stoner criterion says that its magnetic moment should increase. As $x \to 0$ this moment approaches that of an Fe atom.

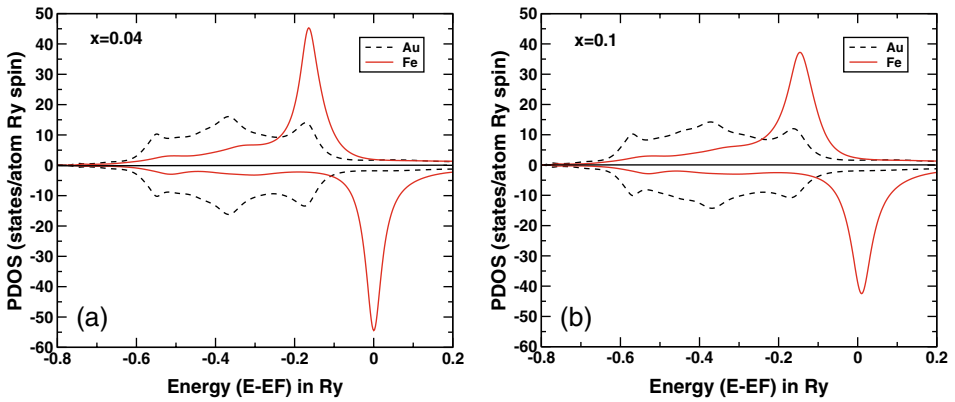

Figure 1. Projected densities of states for Au (dashed line) and Fe (solid line) for $Au_{1-x}Fe_x$ alloys: (**a**) $x = 0.04$ and (**b**) $x = 0.10$.

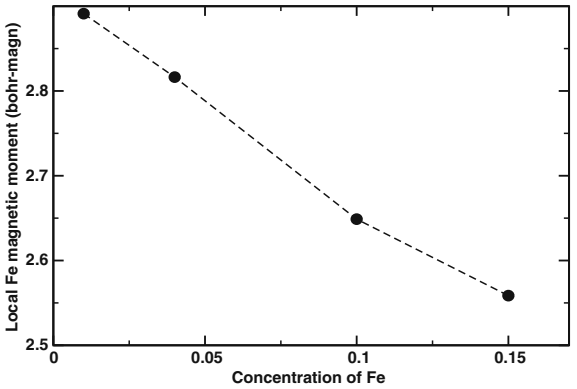

Figure 2. Local magnetic moment at an Fe site in $Au_{1-x}Fe_x$ as a function of Fe concentration x.

Figure 3 shows the atom and spin-projected densities of states for $Ni_{1-x}Mo_x$ at two characteristic compositions: one with low Mo content and the other with a higher one. The electronic structure of NiMo was studied earlier using the CPA by Abrikosov *et al* [22] and using the locally self-consistent Green function (LSGF) by Abrikosov *et al* [23]. We ourselves have earlier studied this alloy system from the point of view of both electronic structure [24] and atomic ordering [25]. Unlike AuFe, the Ni and Mo bands overlap considerably. In addition, unlike Fe, whose magnetism is quite robust, Ni is a fragile magnet whose moment is lost if it is surrounded by too many non-magnetic neighbours. Local magnetic moments on Ni and Mo and the total magnetic moment per atom are shown in figure 4. We see that unlike Au, Mo does carry a magnetic moment in the alloy, although rather small. Also the moment carried by Mo is oppositely oriented to that of Ni. As in all systems in which magnetism is predominantly itinerant, the Mo PDOS becomes narrower as its concentration decreases and its local moment increases. Effect on Ni, however, is rather different. Because of the fragility of its moment, as its concentration

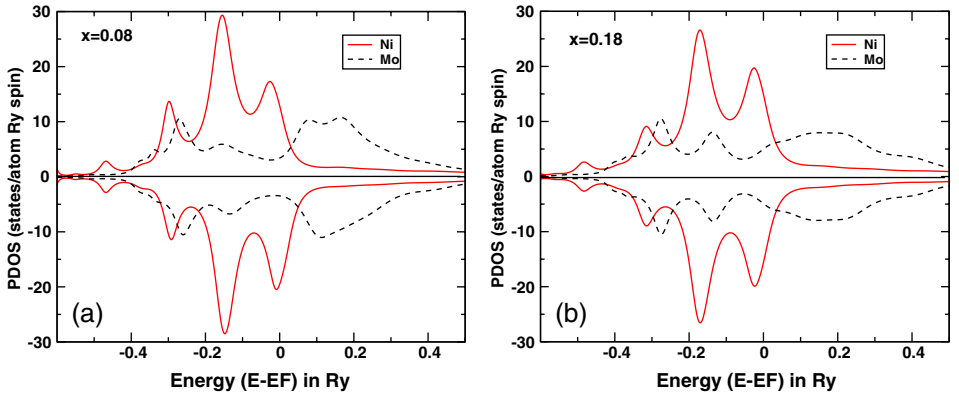

Figure 3. Projected densities of states for Ni (solid line) and Mo (dashed line) in $Ni_{1-x}Mo_x$ alloys: (**a**) $x = 0.08$ and (**b**) $x = 0.18$

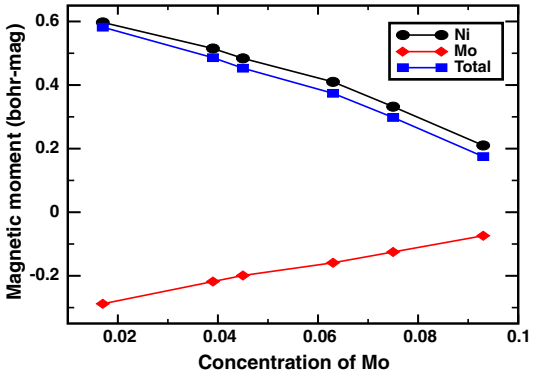

Figure 4. Local magnetic moments at Ni and Mo (AS) sites in $Ni_{1-x}Mo_x$ as a function of Mo concentration x.

decreases and Mo occupying its neighbourhood becomes more probable, Ni moment also decreases. Figure 4 shows that the total magnetic moment of the alloy also decreases as Mo concentration increases and finally vanishes at $x \simeq 0.15$. This is clearly reflected in the experimental data of Asgar *et al* [26]. Spin-glass phase has not been reported in NiMo, although careful experimentation is still required around $x \simeq 0.15$ before Ni loses its local moment.

3. Magnetic ordering and the random Ising model

The analysis of magnetic order from a paramagnetic phase is similar to that of atomic ordering from a chemically disordered phase.

To describe the magnetic phases of an itinerant magnetic alloy we shall follow the generalized perturbation method first introduced by Ducastelle and Gautier [27]. We shall begin with a completely disordered paramagnetic arrangement of atomic spheres each with its own magnetic moment pointing randomly along the quantization direction or opposite to it. Into that system introduce local perturbations and expand the total energies

$$E = E_{\text{dis}} + \sum_{Q,\vec{R}_i} E^{(1),Q}(\vec{R}_i)\delta\xi_i^Q + \frac{1}{2}\sum_{QQ'}\sum_{\vec{R}_i,\vec{R}_j} E^{(2),QQ'}(\vec{R}_i,\vec{R}_j)\delta\xi_i^Q\delta\xi_j^{Q'} \ldots, \quad (3)$$

where Q, Q' are the species of atoms Fe,Ni or Au,Mo. The summation of $\vec{R}_i$ is over those AS occupied by specie Q, and that of $\vec{R}_j$ over AS occupied by specie Q'. The scalar variable $\delta\xi_i^Q$ takes the value ± 1 according to whether the atomic sphere labelled by $\vec{R}_i$ is occupied by a Q specie of atom and its average moment (constructed out of the itinerant electron charge densities as discussed before) points in the quantization direction or opposite to it. Note that $\delta\xi_i^Q$ are *not* spin variables but occupation numbers. Once the averaged magnetic moment in the AS labelled by $\vec{R}_i$ is built up from itinerant electron

densities, the variables $\{\delta\xi_i^Q\}$ can describe how the AS are arranged on the lattice. Consequently, they are scalar, classical variables. Our aim is to determine which arrangement is free-energetically the most favourable.

The terms $E^{(1),Q}(\vec{R}_i)$, $E^{(2),QQ'}(\vec{R}_i, \vec{R}_j)$ are called the renormalized single-site and pair energies. The former plays no role in the ordering of the AS, whereas the higher terms like triplet and quadruplet energies are assumed to be small enough to be ignored. It is easy to note from the above definition that

$$E^{(2),QQ'}(\vec{R}_i, \vec{R}_j) = \frac{1}{2}\sum_{\sigma}\sum_{\sigma'}(2\delta_{\sigma\sigma'} - 1)E^{Q\sigma,Q'\sigma'}_{\vec{R}_i,\vec{R}_j}, \tag{4}$$

where $E^{Q\sigma\,Q'\sigma'}_{\vec{R}_i,\vec{R}_j}$ is the total energy of a paramagnetic background with the sites $\vec{R}_i$ and $\vec{R}_j$ occupied by Q and Q' types of atoms, with σ and σ' the alignments of the averaged magnetic moments in the AS, either along or opposite to the quantization direction. Since $E^{(2),QQ'}(\vec{R}_i, \vec{R}_j)$ are very small energy differences (of the order of mRy) of large energies (of the order of 10^3 Ry), a separate calculation of each component energy will produce errors larger than the small differences themselves. These 'pair energy' parameters will be calculated, following the suggestion by Lichtenstein *et al* [28,29], as

$$\begin{aligned} &E^{(2),QQ'}(\vec{R}_i, \vec{R}_j) \\ &\quad= \frac{1}{4\pi}\int_{-\infty}^{E_F} \mathrm{d}E\ \Im m\ \mathrm{Tr}_L \left\{\underline{\underline{\delta}}^{Q}_{\vec{R}_i}\ \underline{\underline{T}}^{Q\sigma\,Q'\sigma}(\vec{R}_i - \vec{R}_j)\ \underline{\underline{\delta}}^{Q'}_{\vec{R}_j}\underline{\underline{T}}^{Q\sigma'\,Q'\sigma'}(\vec{R}_j - \vec{R}_i)\right\}, \end{aligned} \tag{5}$$

where $\sigma \neq \sigma'$ and $\underline{\underline{\delta}}^{Q}_{\vec{R}_i} = \underline{\underline{P}}^{Q\sigma}_{\vec{R}_i} - \underline{\underline{P}}^{Q'\sigma'}_{\vec{R}_i}$. $\underline{\underline{P}}^{Q\sigma}$ is the on-site potential function of TB-LMTO while $\underline{\underline{T}} = (\underline{\underline{P}} - \underline{\underline{S}})^{-1}$ is the Green operator in a disordered system in which the sites $\vec{R}_i$ and $\vec{R}_j$ are occupied by species $Q\sigma$ and $Q'\sigma'$. $\underline{\underline{S}}$ is the LMTO structure matrix. We should note that these energy calculations are also from an itinerant electron viewpoint.

Figure 5a shows the variation of $J(R) = E^{(2),\mathrm{FeFe}}(R)$ with R for various compositions of the $Au_{1-x}Fe_x$ alloy. We may note two features of the pair energies:

(i) The pair energies are dependent on the composition. The simplified models without exception assumed that the pair energy depended only on the materials comprising the alloy. The right panel of figure 5b shows the composition dependence of $J_n = J(R_n)$ at various values of nth neighbour distance R_n on the face-centred cubic lattice. Both J_1 and J_2 show strong dependence on the Fe concentration x. Several pair energies (markedly J_2) change their sign with increasing Fe concentration. This has to be incorporated in any realistic model of the spin-glass.

(ii) The pair energy $J(R)$ oscillates in sign with increasing R so that the possibility of frustration is present. The nearest-neighbour pair energy is strongly ferromagnetic and quite a bit larger than the next-nearest-neighbour one. The pair energies exhibit exponential decay characteristic of disorder damping. With increasing Fe concentration, disorder scattering increases and so does the damping. A model with damped, oscillatory interaction seems suitable for these alloys.

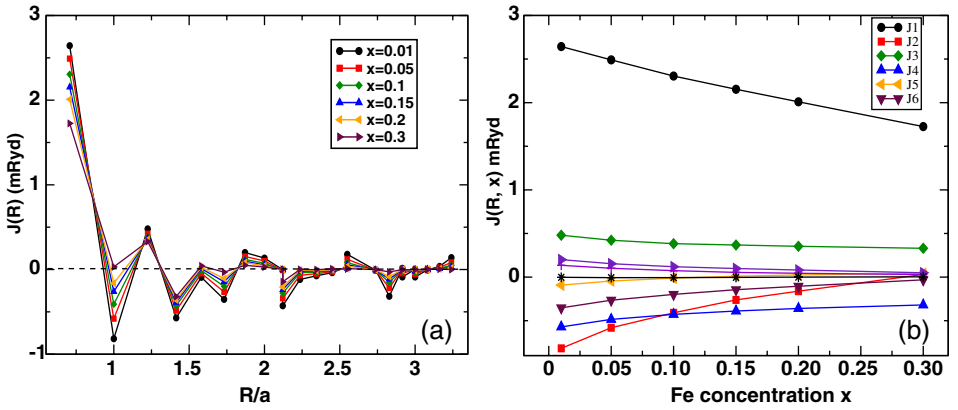

Figure 5. (**a**) The pair energy $J^{\mathrm{FeFe}}(R)$ for AuFe alloys, across the composition range, as a function of $R = |\vec{R}_i - \vec{R}_j|$. (**b**) Variation of $J^{\mathrm{FeFe}}(R)$ with composition.

Let us examine the behaviour of $J(R)$ in greater detail. To quantify the variation of J_n with n we use the spatial moments of the scaled pair energy

$$I_0 = \sum_R W(R)J(R)$$
$$I_{n-1} = \sum_{R \geq a} W(R)\{J(R)/I_0\}^n, \quad n = 2, 3, \ldots, \tag{6}$$

where $W(R)$ are the coordination numbers on the face-centred cubic lattice.

From figure 6 we note that the third and fifth moments I_2 and I_4 are negative which are the characteristics of distribution which are asymmetric with more weightage towards negative or antiferromagnetic pair energies. This asymmetry decreases as the concentration of Fe increases and at around $x \simeq 0.16$–0.18 the moments become positive. The fourth moment I_3 goes to zero with increasing x indicating that the distribution becomes more Gaussian, while the second moment I_1 also decreases and the distribution about the mean becomes sharp delta function-like. Can these results throw some light on the nature of frustration in the system and its behaviour with x? Khmelevskyi *et al* [31] used the partial moments $K(R_0) = \sum_{R>R_0} W(R)J(R)$ to illustrate frustration. We argue that the moments by themselves cannot give full information about frustration unless we couple them with the lattice topology. Predominance of antiferromagnetic pair energies indicates the possibility of frustration. But antiferromagnetic pair energies themselves may not lead to frustration until we couple it to frustrated plaquettes on the lattice. On bipartite lattices even completely antiferromagnetic pair energies lead to no frustration at all.

Figure 7 shows the smallest triangular and quadrilateral plaquettes within a cubic unit cell of the face-centred cubic lattice. Only one example (figure 7f) covers a triangular plaquette that spans two neighbouring cells. The signs shown are that of the corresponding $J(R)$ for $x = 0.01$. All these plaquettes involve sides which are up to fifth nearest-neighbours. Given the exponential decay of $J(R)$ with R, these smaller plaquettes are energetically the most important. The nearest-neighbour plaquette (figure 7a) is

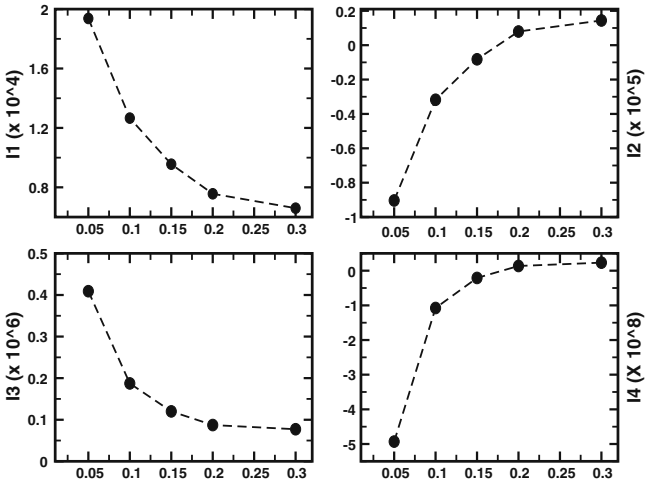

Figure 6. Moments of $J(R)$ for AuFe alloys (for $R \geq a$) and their variation with composition.

not frustrated, as all pair energies are ferromagnetic. All the remaining triangular plaquettes (figures 7b–f) are frustrated. However, as $x \geq 0.16$ both the second and fifth nearest-neighbour pair energies change sign and all these plaquettes lose their frustration.

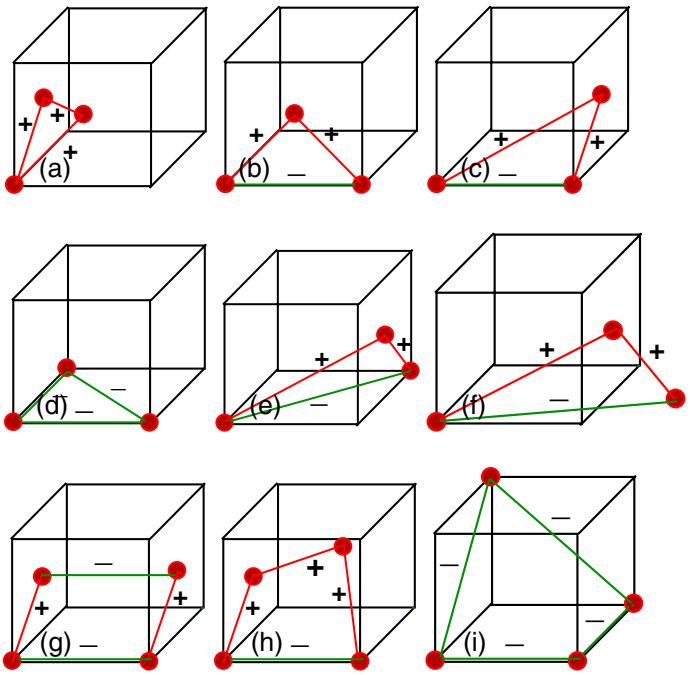

Figure 7. Plaquettes on the face-centred cubic lattice. Signs are those of the corresponding pair energies for $x = 0.01$.

In the bottom row, the quadrilaterals (figures 7h and 7i) are also frustrated at $x = 0.01$ and lose their frustration as $x \geq 0.16$ and the second and the fifth nearest-neighbour pair energies change sign. Table 1 shows the statistics of the plaquettes of various sizes and shapes within the cubic unit cell. When the concentration of Fe increases, 78% of the triangular and 90% of the polygonal plaquettes which were frustrated earlier lose their frustration.

It is clear from the examination of the smaller plaquettes on a face-centred cubic lattice that the degree of frustration, as measured by the number of frustrated plaquettes, decreases considerably as x increases. Since frustration is central to the understanding of the spin-glass, the decrease of the degree of frustration with increasing x could be understood as the cause of the spin-glass to random ferromagnet transition with composition at $T = 0$. This could not have been understood without a microscopic derivation of the coupling.

We shall now turn to the NiMo alloy. Unlike AuFe, where alloying with Fe still leaves the Au atoms with negligible moment, in NiMo, Mo gains a small moment and the pair energy between Ni and Mo and Mo and Mo are not negligible. Figure 8 shows these pair energies as functions of distance. The Ni–Ni pair energy in NiMo has significant differences from the Fe–Fe pair energy in AuFe. Although the nearest-neighbour pair energy is still ferromagnetic, the antiferromagnetic second-nearest-neighbour pair energy is very small and dominated by the ferromagnetic third-nearest-neighbour one. Both the Ni–Ni and Ni–Mo pair energies show the characteristic decay due to disorder scattering. The Ni–Mo pair energy is ferromagnetic, but at low Mo concentrations most of the neighbours of Ni are also Ni. It is more probable to find mO at the next-nearest-neighbour positions. The relatively large next-nearest-neighbour antiferromagnetic Ni–Mo pair energies may then explain why the Mo and Ni atoms have moments antiparallely aligned.

However, a look at figure 9 shows that unlike AuFe, the moments of $J^{\mathrm{NiNi}}(R)$ are all positive and strongly decrease as x increases. As for AuFe in NiMo too the local 'Weiss' field has a distribution which becomes more Gaussian as x increases and increasingly sharp. The positive sign of the third and fifth moments indicate that the pair energies are predominantly ferromagnetic. This means that frustration is negligible exactly in the compositions where spin-glass may become possible. This, coupled with the fact that exactly in this region the Ni atoms lose their local moments, may be the reason why spin-glass phase has not been observed in NiMo.

A comment must be made regarding the oscillatory pair energies in these alloy systems. Ling *et al* [32] have discussed the pair energies in CuMn, another spin-glass alloy. They argued that if the Fermi energy straddled the local DOS peak of the magnetic component, then ferromagnetism was favoured, whereas antiferromagnetism was stabilized if the local DOS peaks were away from the Fermi energy. In CuMn, the t_{2g} states are more nearly filled and provoke a ferromagnetic tendency whereas the e_g states being away from the

Table 1. Number of different triangular, quadrilateral and pentagonal plaquettes in a cubic unit cell.

Plaquette	(a)	(b)	(c)	(d)	(e)	(g)	(h)	(i)
Number	32	24	24	24	48	12	72	48

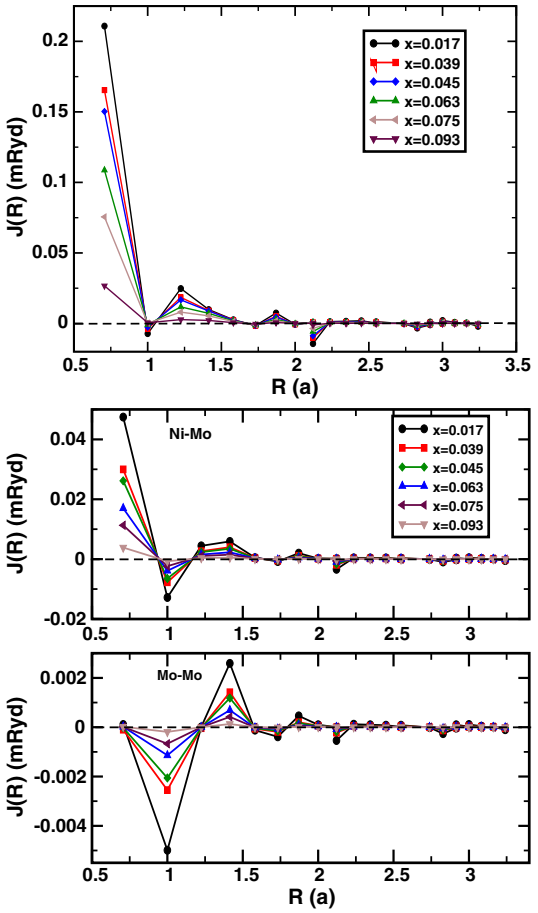

Figure 8. Pair energies $J(R) = E^{(2)QQ'}(R)$ for Q, Q' (top) Ni–Ni, (middle) Ni–Mo and (bottom) Mo–Mo in $Ni_{1-x}Mo_x$.

Fermi energy stabilizes antiferromagnetism. The competition between these two tendencies suppresses direct magnetic interactions between the magnetic atoms and enhances the role of indirect interactions. The outcome is the interpretation of magnetic interactions in terms of damped, oscillatory RKKY-like interactions. This may not be reflective of actual RKKY interactions. The authors themselves argue that a similar conclusion is possible for AuFe alloys. Here the Au DOS forms the paramagnetic background on which the Fe DOS forms the 'virtual bound states' as shown in figure 1. For NiMo too, a similar argument can be made. A look at the Ni projected DOS shown in figure 3 shows that the e_g and t_{2g} structures in the DOS are well separated: one straddling the Fermi energy and the other away from it.

The physics of the interplay between chemical and magnetic orderings in AuFe was described in some detail by Ling *et al* [33]. The authors used the KKR-CPA-type calculations to obtain the Ornstein–Zernicke direct correlation function from the electronic grand

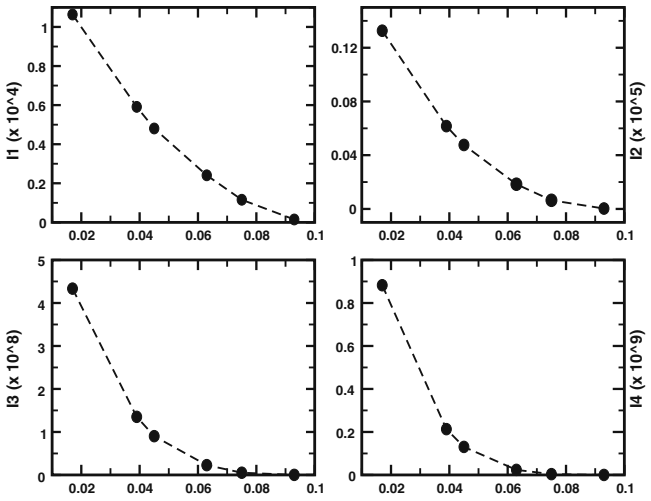

Figure 9. Spread of $J^{\mathrm{NiNi}}(R)$, $R \geq a$ with R for different compositions of NiMo.

potential. In this paper we have not addressed the problem of chemical ordering and its effect on magnetic ordering. The Ising model which we have set up is obtained, from a generalized perturbation, by introducing magnetic fluctuations in an otherwise non-magnetic background. Tahir-Kheli and Kawasaki [34] have introduced an Ising model which arose via a generalized perturbation approach when we introduced both magnetic and composition fluctuations in an otherwise paramagnetic, chemically disordered background. We propose to study such a model in future.

4. Phase analysis of AuFe and NiMo

Our model consisted of N_A, A and N_B, B atoms uniformly distributed over M lattice sites and interacting through our estimated pair energies $J(|\vec{R}_i - \vec{R}_j|)$. These may vary in sign as a function of distance providing the main ingredient, frustration, in the system. The probability of an atom A occupying a specific site $\vec{R}_k$ is $1/M$, as every site has equal probability of occupation. Similarly, the probability that a site is occupied by a A atom is N_A/M and a B atom is N_B/M. In the thermodynamic limit, in the absence of any clustering or segregating effects

$$\lim_{N_A, M\to\infty} \frac{N_A}{M} = x_A, \qquad \lim_{N_B, M\to\infty} \frac{N_B}{M} = x_B$$

x_A, x_B being the atomic concentrations of A and B constituents. The random 'Hamiltonian' is the same as shown in eq. (3):

$$\Delta E = \frac{1}{2} \sum_{QQ'} \sum_{\vec{R}_i, \vec{R}_j} J^{QQ'}(|\vec{R}_i - \vec{R}_j|)\, \delta\xi_i^{Q} \delta\xi_j^{Q'},$$

where

$$J^{QQ'}(R) = E^{(2),QQ'}(R).$$

For a binary alloy, Q, Q' can be either A or B. $J^{QQ'}(|R_i - R_j|)$ is random depending on which type of atoms occupy the sites R_i and R_j. It can take on the values $J^{AA}(|R_i - R_j|)$, $J^{BB}(|R_i - R_j|)$ or $J^{AB}(|R_i - R_j|)$.

Introducing the single-site mean-field approach by replacing the quadratic term $\delta\xi_i^Q \delta\xi_j^{Q'}$ by $\delta\xi_i^Q m_j^{Q'} + \delta\xi_j^{Q'} m_i^Q - m_i^Q m_j^{Q'}$, where m_i^Q is the thermal average $\langle \delta\xi_i^Q \rangle$, we can obtain the free energy as

$$F = -\frac{1}{2} \sum_{QQ'} \sum_{R_j, R_j \in QQ'} J^{QQ'}(|R_i - R_j|) m_i^Q m_j^{Q'} + \frac{1}{\beta} \sum_Q \sum_{\vec{R}_i \in Q} \log\cosh(\beta h_i^Q), \tag{7}$$

where the local 'Weiss' fields are

$$h_i^Q = \sum_{Q'} \sum_{R_j \in Q'} J^{QQ'}(|R_i - R_j|) m_j^{Q'}. \tag{8}$$

In an ordered alloy we can define a homogeneous order parameter corresponding to the occupation variable of a Q type of atom as $m^Q = (1/N_Q) \sum_{i \in Q} m_i^Q$ and an average global order parameter as $m = \sum_Q x_Q m^Q$. In our disordered system, inhomogeneities are in a macroscopic scale and this prevents us from introducing such an idea prior to some kind of configuration averaging. Rather we picture the system as follows: the net result of random pair energies connecting a local order parameter with its neighbourhood is that it experiences a local random 'Weiss' field along which the average AS moment aligns. This leads to a *set of local order parameters* $\{m_i^Q\}$. To describe the local order parameters we need to know the distribution of the local 'Weiss' fields. This interpretation links our work with that of Thouless [7] and Mookerjee [35]. The free energy is a function of the whole set of local order parameters. The stable phase solution comes from the equations $\partial F / \partial m_i^Q = 0$ for all i. This leads to

$$m_j^Q = \tanh\left[\beta h_j^Q\right], \quad Q, Q' \text{ can be } A \text{ or } B. \tag{9}$$

For sufficiently high temperatures, the only consistent solution will be $m_i^Q = 0\ \forall i$. At low concentrations of the magnetic constituent and as we lower the temperatures, some of the local order parameters become non-zero and they are distributed randomly on the lattice. As many of them are '+' as they are '−', the net global order parameter may be zero, but the local one is still non-zero but random at Fe atoms. Moreover, there could be several different configurations of ± order parameters which have the same free energy. This implies that rather than having a unique stable phase with non-zero global order parameter, we have a very corrugated free energy landscape with many minima differing in random distributions of ± moment carrying AS separated from each other by energy barriers. The resulting 'phase' may consist of domains with differing local AS configurations. One way of describing such an inhomogeneous picture is to find the distribution function of the scaled local 'Weiss' field. The scaling is carried out as follows: $J(R)$ is replaced by $I(R) = J(R)/I_0$. If there is only one magnetic constituent, the scaling is done with $I_0 = \sum_R W(R) J(R)$. If both the constituents are magnetic we have three factors

I_0^{AA}, I_0^{AB} and I_0^{BB} and we scale with respect to $I_0 = \max\{I_0^{AA}, I_0^{AB}, I_0^{BB}\}$. Here $W(R)$ is the coordination number at a distance R from an origin.

The scaled 'Weiss' fields are given by

$$\hat{h}_i^Q = \sum_{Q'} \sum_{R_j \in Q'} I^{QQ'}(|R_i - R_j|) m_j^{Q'}.$$

The technique for the derivation of distribution function was described earlier by Klein [36] and Mookerjee [35] and the reader is referred to those papers for details. Here we shall quote the procedure and the main results. The probability is first expressed as a radon transform of eq. (8) and then the approximation is introduced in which we replace the delta-functional kernel of the radon transform by its configuration average. Under the assumption that local 'Weiss' fields at different sites are uncorrelated, so that there is no clustering or short-ranged correlations between the local order parameters, we get

$$\mathcal{P}_Q(\hat{h}_i^Q) = \frac{1}{2\pi} \int \mathrm{d}k \, \mathrm{e}^{ik\hat{h}_i^Q} \prod_{Q'} \left[1 - \frac{F_{QQ'}(k)}{M}\right]^{N_{Q'}},$$

where

$$F_{QQ'}(k) = \sum_R \int \mathrm{d}z \mathcal{P}_Q(z) \big[1 - \exp\big\{ - ikI^{QQ'}(R) \tanh(\beta J^{QQ'}(R) z)\big\}\big].$$

In the thermodynamic limit

$$\mathcal{P}_Q(\hat{h}_i^Q) = \frac{1}{2\pi} \int \mathrm{d}k \exp\big\{ik\hat{h}_i^Q - \sum_{Q'} x_{Q'} F_{QQ'}(k)\big\}.$$

The direct calculations of $F_{QQ'}(k)$ are tough as it stands, but let us expand the exponential and examine the terms

$$F_{QQ'}(k) = \int \mathrm{d}z \, \mathcal{P}_Q(z) \Bigg[ikI_0^{QQ'} \tanh(\beta J_0^Q z) + \frac{k^2}{2} I_1^{QQ'} \tanh^2(\beta J_0^Q z) \ldots + \frac{(-ik)^3}{6} I_2^{QQ'} \tanh^3(\beta J_0^Q z) \ldots \Bigg],$$

where

$$\sum_R W(R) I^n(R) = I_{n-1}, \qquad n = 1, 2, \ldots.$$

We define

$$J_0^Q = \sum_{Q'} x_{Q'} m^{Q'} \sum_R J^{QQ'}(R) = \sum_{Q'} k_\mathrm{B} T_{QQ'} m^{Q'},$$

$$J_1^Q = \sum_{Q'} x_{Q'} q^{Q'} \sum_R J^{QQ'}(R)^2 = \sum_{Q'} k_\mathrm{B}^2 T^{g2}_{QQ'} q^{Q'}$$

and

$$m^Q = \int \mathrm{d}z\, \mathcal{P}_Q(z)\, \tanh(\beta J_0^Q z),$$
$$q^Q = \int \mathrm{d}z\, \mathcal{P}_Q(z)\, \tanh^2(\beta J_0^Q z). \tag{10}$$

Comparing eqs (9) and (10), we note that we can interpret m^Q and q^Q as the configuration averages $\langle\langle m_i^Q\rangle\rangle$ and $\langle\langle (m_i^Q)^2\rangle\rangle$. Our frozen disordered local moment picture envisages spin-glass in AuFe as a ternary alloy $\mathrm{Au}_{1-x}\mathrm{Fe}^{\uparrow}_{x/2}\mathrm{Fe}^{\downarrow}_{x/2}$, and that in NiMo as a quaternary alloy $\mathrm{Ni}^{\uparrow}_{1-x/2}\mathrm{Ni}^{\downarrow}_{1-x/2}\mathrm{Mo}^{\uparrow}_{x/2}\mathrm{Mo}^{\downarrow}_{x/2}$. For this phase $m^Q = 0$, but $q^Q \neq 0$. Thus the frozen disordered moment picture is consistent with our model for a spin-glass.

From figure 10 we see that the moments I_{n-1} rapidly decrease as n increases. We shall therefore neglect all terms with I_{n-1} with $n > 3$. Then the probability densities become Gaussian. The distribution of the unscaled local 'Weiss' field $h = J_0\,\hat{h}$ becomes

$$\mathcal{P}_Q(h^Q) = \frac{1}{\sqrt{2\pi J_1^Q}} \exp\{-(h^Q - J_0^Q)^2/(2J_1^Q)\}.$$

Equations (10) then reduce to the standard mean-field equations

$$m^Q = \frac{1}{\sqrt{2\pi}} \int \mathrm{d}z\, \mathrm{e}^{-z^2/2} \tanh\left[\sum_{Q'} \frac{T_{QQ'}}{T} m^{Q'} + \frac{T^{g2}_{QQ'}}{T^2} q^{Q'} z\right],$$
$$q^Q = \frac{1}{\sqrt{2\pi}} \int \mathrm{d}z\, \mathrm{e}^{-z^2/2} \tanh^2\left[\sum_{Q'} \frac{T_{QQ'}}{T} m^{Q'} + \frac{T^{g2}_{QQ'}}{T^2} q^{Q'} z\right].$$

The results are similar to many earlier work based on the distribution of local 'Weiss' fields, but it must be emphasized that our derivation has made assumptions that take into

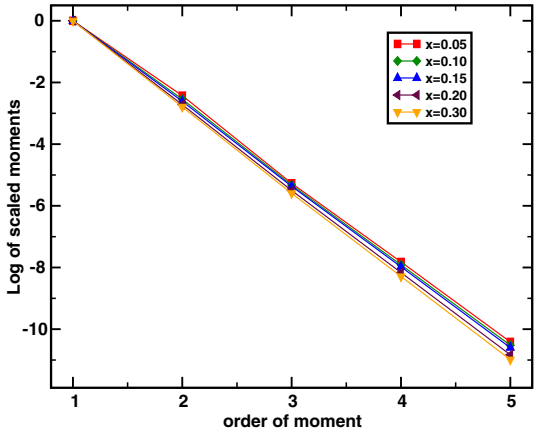

Figure 10. Decay of scaled moments I_n with n for AuFe.

account both a correct description of substitutional disorder and correct form of the pair energies. The scaling of both the mean and variance of the local 'Weiss' field with concentration of the magnetic component naturally arises in our results. Moreover, in this derivation we emphasize the distribution of local 'Weiss' fields, so that the inhomogeneous picture of the system remains intact. m^A, m^B, q^A, q^B are being related to the moments of the local 'Weiss' field distribution.

One phase is characterized by $m^Q = 0$, $q^Q = 0$ so that the 'Weiss' field distribution is a delta function at $h^Q = 0$. This is obviously a paramagnetic phase with no local or global magnetization. Another phase is characterized by $m^A = 0, m^B = 0, q^A \neq 0, q^B \neq 0$. Here the distributions of the 'Weiss' fields are Gaussian with means at zero but with a non-zero spread. How can such a phase be described? As the mean is zero, the local magnetization is positive at as many sites as it is negative. This is exactly the frozen disordered moment picture described earlier. The spin-glass phase boundary is given by

$$T_g = \frac{1}{2}\left\{(T^g_{AA} + T^g_{BB}) + \sqrt{(T^g_{AA} - T^g_{BB})^2 + 4T^g_{AB}T^g_{BA}}\right\}. \tag{11}$$

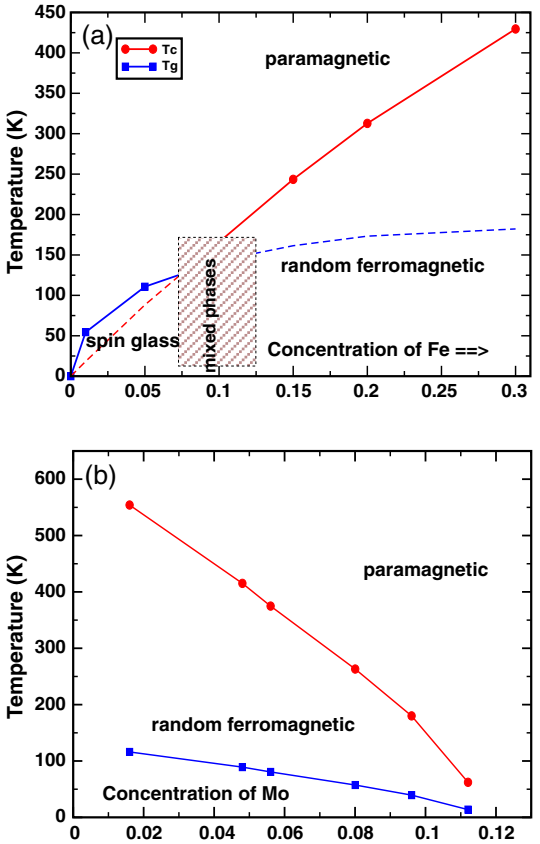

Figure 11. Phase diagrams for (**a**) AuFe and (**b**) NiMo alloys.

If one of the constituents is non-magnetic, so that $J^{AB} = J^{BA} = J^{BB} = 0$, $J^{AA} \neq 0$ and $x_A = x$, $x_B = 1 - x$, as in the case of AuFe, then

$$k_{\mathrm{B}} T_g(x) = \sqrt{x J_1^A(x)}. \tag{12}$$

Finally there is a third phase where $m^A \neq 0,\ m^B \neq 0,\ q^A \neq 0,\ q^B \neq 0$. For this phase the distributions of the local 'Weiss' fields are shifted Gaussians with a non-zero mean. So there is a distribution of different local moments as also the global averaged moment is non-zero. This is the random ferromagnetic phase. This boundary is given by

$$T_c = \frac{1}{2}\left\{T_{AA} + T_{BB} + \sqrt{(T_{AA} - T_{BB})^2 + 4T_{AB}T_{BA})}\right\}. \tag{13}$$

For only one magnetic constituent, as in AuFe, we get

$$k_{\mathrm{B}} T_c(x) = x J_0^A(x). \tag{14}$$

The derivation of the distribution of the local 'Weiss' fields in alloys with both components carrying moments was done in detail earlier and we refer the reader to the work of Mookerjee and Roy [37]. Figure 11a shows the phase boundaries between the paramagnetic, random ferromagnetic and spin-glass phases for AuFe. As we have seen that Au carries negligible local moment, we have used eqs (12) and (14). The range in the concentration–temperature domain where we have the possibility of clustering and mixed phases has been blocked out, as our simple mean-field theory cannot hope to describe such phenomena. If we compare the phase diagram with experiment, qualitative agreement is immediately observed [38]. Since this is a mean-field theory, we do not expect very good agreement quantitatively. However, the overall trend is well reproduced.

Figure 11b plots similar phase boundaries for NiMo. As both the constituents carry moment, we shall use the more general eqs (11) and (13). The paramagnetic–random ferromagnetic boundary agrees very well with the experimental results of Asgar *et al* [26]. We note that in most of the temperature–concentration domain the spin-glass boundary lies well below the random ferromagnetic one. Only in a small region around 11–13% Mo concentration (atomic) is there a possibility of these boundaries to cross and a possibility of spin-glass transition.

Acknowledgments

BS and RB acknowledge financial support from Guest Scholarship Programme of Swedish Institute. Supercomputing facilities allotted by Swedish National Infrastructure for Computing (SNIC) and UPPMAX computing facilities are gratefully acknowledged.

References

[1] J A Mydosh, *Spin glasses: An experimental introduction* (Taylor & Francis, London, 1993)
[2] S Kirkpatrick and D Sherrington, *Phys. Rev.* **B17**, 4384 (1978)
[3] G Parisi, *Phys. Rev. Lett.* **50**, 1946 (1983)
[4] M Mezard, G Parisi and M A Virasoro, *Spin-glass theory and beyond* (Springer Lecture Series, 1983)

[5] T Kaneyoshi, *J. Phys. C: Solid State Phys.* **9**, L289 (1976)
[6] T Plefka, *J. Phys. F: Metal Phys.* **6**, L327 (1976)
[7] D J Thouless, P W Anderson and Palmer, *Phil. Mag.* **35**, 593 (1977)
[8] T Morita and T Horiguchi, *Solid State Commun.* **19**, 833 (1975)
[9] A Larkin and A Khmelnitskii, *JETP Sov. Phys.* **31**, 958 (1970)
[10] O K Andersen and O Jepsen, *Phys. Rev. Lett.* **53**, 2571 (1984)
[11] K Tarafder, S Ghosh, B Sanyal, O Eriksson, A Mookerjee and A Charkrabarti, *J. Phys.: Condens. Matter* **20**, 445201 (2008)
[12] A Mookerjee, in: *Electronic structure of alloys, surfaces and clusters* edited by D D Sarma and A Mookerjee (Taylor-Francis, UK, 2003)
[13] V Kumar, V K Srivastava and A Mookerjee, *J. Phys. C: Solid State Phys.* **15**, 1939 (1982)
[14] A Mookerjee and R Prasad, *Phys. Rev.* **B48**, 17724 (1993)
[15] T Saha, I Dasgupta and A Mookerjee, *Phys. Rev.* **B50**, 13267 (1994)
[16] T Saha and A Mookerjee, *J. Phys.: Condens. Matter* **8**, 2915 (1996)
[17] R Haydock, in: *Solid state physics* (Academic Press, New York, 1980) Vol. 35
[18] N Beer and D Pettifor, in: *The electronic structure of complex systems* (Plenum Press, New York, 1984)
[19] A V Ruban and H L Skriver, *Phys. Rev.* **B66**, 024201 (2002)
[20] A V Ruban, S Shallcross, S I Simak and H L Skriver, *Phys. Rev.* **B70**, 125115 (2004)
[21] T Saha and A Mookerjee, *J. Phys.: Condens. Matter* **9**, 6607 (1997)
[22] I A Abrikosov, S I Simak, B Johansson, A V Ruban and H L Skriver, *Phys. Rev.* **B56**, 9319 (1997)
[23] I A Abrikosov, A M N Niklasson, S I Simak, B Johansson, A V Ruban and H L Skriver, *Phys. Rev. Lett.* **76**, 4203 (1996)
[24] S Ghosh, N Das and A Mookerjee, *J. Phys.: Condens. Matter* **10**, 11773 (1998)
[25] A Arya, S Banerjee, G P Das, I Dasgupta, T Saha-Dasgupta and A Mookerjee, *Acta Mater.* **49**, 3575 (2001)
[26] A F Asgar, M A Khan and P Nordblad, *J. Magn. Magn. Mater.* **174**, 121 (1997)
[27] F Ducastelle and F Gautier, *J. Phys. F: Metal Phys.* **6**, 2039 (1976)
[28] A I Lichtenstein, M I Katsnelson, V P Antropov and V A Gubanov, *J. Magn. Magn. Mater.* **67**, 65 (1987)
[29] A I Lichtenstein, A P Andropov and V A Gubanov, *Phys. Met. Metallogr.* **64(4)**, 35 (1987)
[30] A Sakuma, *J. Phys. Soc. (Japan)* **68**, 620 (1998)
[31] S Khmelevskyi, J Kudrnovský, B L Gyorffy, P Mohn, V Drchal and P Weinberger, *Phys. Rev.* **B70**, 224432 (2004)
[32] M F Ling, J B Staunton and D D Johnson, *Europhys. Lett.* **25**, 631 (1994)
[33] M F Ling, J B Staunton, D D Johnson and F J Pinski, *Phys. Rev.* **B52**, R3816 (1995)
[34] R A Tahir-Kheli and T Kawasaki, *J. Phys. C: Solid State Phys.* **10**, 2207 (1977)
[35] A Mookerjee, *Pramana – J. Phys.* **11**, 223 (1978)
[36] M Klein, *Phys. Rev.* **B173**, 552 (1968)
[37] A Mookerjee and S B Roy, *Pramana – J. Phys.* **21**, 171 (1983)
[38] B V B Sarkissian, *J. Phys. F: Metal Phys.* **11**, 2191 (1981)